

Stable components of sound fields in the ocean

A.L. Virovlyansky

Institute of Applied Physics, Russian Academy of Science

46 Ul'yanov Street, 603950 Nizhny Novgorod, Russia

Abstract

A method is proposed for finding the wave field components which are weakly sensitive to the sound speed perturbation in the ocean acoustic waveguides. Such a component is formed by a narrow beam of rays whose spread in vertical direction, up to the observation range, remains less than the vertical scale of perturbation. These rays pass through practically the same inhomogeneities and therefore their phases acquire close increments. If the ray amplitudes vary insignificantly, then (i) the stable component of the monochromatic field in the perturbed and unperturbed waveguide differ by only a constant phase factor, and (ii) in the case of transient wave field the perturbation causes only an additional time delay of the stable component as a whole. It is shown how the stable components can be selected from the total wave field using the field expansions in coherent states or in normal modes. The existence of stable components is demonstrated by numerical simulation of sound field in a deep water waveguide. It turns out, that even though the assumptions (i) and (ii) are not met exactly, the stable components in the perturbed and unperturbed waveguide are quite close.

PACS number(s): 43.30.Cq, 43.30.Bp, 43.30.Re

I Introduction

The main factor reducing the accuracy of field simulation in the ocean acoustic waveguide is the inevitable inaccuracy of environmental model used in solving the wave equation. When analyzing this issue, the main attention is usually paid to questions on how the uncertainty in environmental parameters manifests itself in field predictions [1, 2] and in solutions of inverse problems [3, 4]. This work is devoted to another aspect of the problem of inaccurate knowledge of the environment model. We argue that at relatively short ranges there exist such components of the wave field which are weakly sensitive to the variations of waveguide parameters and can be predicted with a reasonable accuracy even under conditions of uncertain environment.

For the analysis of field variations caused by a weak sound speed perturbation we use the geometrical optics approximation. The geometrical-optics description takes especially simple form at short ranges where the deviation of ray path from its unperturbed position caused by the perturbation is negligible [5, 6]. At these range the ray amplitude remains almost the same and its phase acquires an increment ϕ , which, generally, is not small and can exceed π . The object of our study is a component of the total field formed by a narrow beam of rays escaping a point source at close launch angles. As long as the spread of ray paths along the vertical coordinate remains small compared to the vertical scale of perturbation all the rays pass through practically the same inhomogeneities and their phase increments vary synchronously. At ranges where the phase increments ϕ of these rays are almost the same, the beam forms a component of the total field which we call stable. Its stability manifests itself as follows. (i) In the presence of perturbation this component is multiplied by a phase factor $e^{i\phi}$, where ϕ (it is not assumed to be small) depends on the perturbation and range but does not depend on the depth. (ii) If the source emits a pulse signal, then this beam of rays forms a stable component of the transient field. In the presence of perturbation this component acquires only an additional depth-independent time delay.

The so-determined stable component of the total field at the range of observation is formed by rays arriving at close grazing angles into a small depth interval. In terms of the Hamiltonian formalism these rays arrive at a small area of the phase plane. We say that the stable component is associated with this area.

Our objective is to extract the stable component from the total field. To solve this problem, two methods are proposed. One of them is based on using the coherent state

formalism borrowed from quantum mechanics. Another method is based on the modal representation of the wave field. The use of these instruments is explained by the fact that the coherent state and normal mode describe the components of the wave field formed by contributions of rays from small cells of the phase plane. These cells have different shapes but equal areas.

The existence of stable components is demonstrated by numerical simulation on an example of a deep-water waveguide. We compare sound field components formed by the same beam of rays in the unperturbed waveguide and in the presence of sound speed fluctuations. Their closeness is characterized by a quantitative criterium. It turns out that even though the conditions (i) and (ii) are not met exactly the stable components in the perturbed and unperturbed waveguide are quite close.

The paper is organized as follows. Heuristic arguments on the existence of stable components of the sound field formed by narrow beams of rays are presented in Sec. II. Section III describes a model of the waveguide, which is then used to illustrate and test the results. Procedures for construction of stable components from coherent states and normal modes are formulated in Secs. IV and V, respectively. Section VI presents the numerical evidences confirming the existence of stable components. In Sec. VII the results of this work are summarized.

II Heuristic arguments for the existence of stable components

Neglecting horizontal refraction, we consider a sound field at a carrier frequency f in a waveguide with the sound speed $c(r, z)$, where r is the range and z is the depth. The refractive index is $n(r, z) = c_0/c(r, z)$, where c_0 is the reference sound speed satisfying condition $|c(r, z) - c_0| \ll c_0$. In what follows we assume that the sound field is excited by a source set at point $(0, z_s)$.

In the geometrical optics approximation the wave field at the observation point is formed by contributions from eigenrays arriving at this point. The contribution from a single eigenray is $A \exp(ikS)$, where A and S are the ray amplitude and eikonal, respectively, $k = 2\pi f/c_0$ is the reference wave number. In the presence of a weak sound speed perturbation $\delta c(r, z)$, the deviation of a ray path from its unperturbed position at short ranges can be

neglected. Then the influence of perturbation can be accounted for by replacing $A \exp(ikS)$ with $A \exp(ik(S + \delta S))$, where

$$\delta S = -\frac{1}{c_0^2} \int_{\Gamma} ds \delta c, \quad (1)$$

Γ is the unperturbed ray path, and ds is the arc length [5, 6]. This approximate formula is widely used in underwater acoustics. In a deep ocean at frequencies of order 100 Hz it is applied at ranges up to a few hundred kilometers [5].

In the scope of Hamiltonian formalism the ray path at range r is determined by its vertical coordinate z and momentum $p = n(r, z) \sin \chi$, where χ is the ray grazing angle [7]. The path is described by functions $p(r, p_0, z_0)$ and $z(r, p_0, z_0)$, where p_0 and z_0 are the starting momentum and coordinate at $r = 0$, respectively.

Consider a beam of ray paths leaving the source with starting momenta in an interval $p_0 \pm \delta p_0/2$. If δp_0 is so small that the spread of ray coordinates z at any range $r' < r$ is small compared to the vertical scale of perturbation δc , then it may be expected that at range r phase increments $k\delta S$ of all these rays are almost the same, that is, their differences are small compared to π . It should be emphasized that $k|\delta S|$ is not assumed to be small and it can exceed π . Below we will call such rays the rays with close phase increments.

At the observation range r the contributions of these rays form a component of the total wave field whose complex amplitude in the vertical section we denote $u_s(z)$. It is defined only at arrival depths of beam rays. The component of the sound field formed by the same rays in the unperturbed waveguide denote $\tilde{u}_s(z)$. Since the phase increments $k\delta S$ of all beam rays are close

$$u_s(z) = e^{ik\delta S} \tilde{u}_s(z). \quad (2)$$

The closeness of functions $u_s(z)$ and $\tilde{u}_s(z)$ can be quantitatively characterized by the similarity coefficient

$$B_{\text{cw}}(u_s, \tilde{u}_s) = \frac{|\int dz u_s(z) \tilde{u}_s^*(z)|}{(\int dz |u_s(z)|^2)^{1/2} (\int dz |\tilde{u}_s(z)|^2)^{1/2}}, \quad (3)$$

where the asterisk denotes complex conjugation (in quantum mechanics a similar characteristic is called fidelity). If the depth dependence of phase increment $k\delta S$ is weak, then the similarity coefficient B is close to unity and we call $u_s(z)$ a stable component of the total field.

If the source emits a pulse signal

$$s(t) = \int df g(f) e^{-2\pi i f t}, \quad (4)$$

where t is the time, then the transient sound field at the observation range r is

$$v(z, t) = \int df g(f) u(z, f) e^{-2\pi i f t}, \quad (5)$$

where $u(z, f)$ is a monochromatic field excited by the source at frequency f . Consider a beam of rays whose increments at the observation range are close at all frequencies within the signal bandwidth. At each of these frequencies the beam forms a stable components $u_s(z, f)$ of $u(z, f)$. We will call

$$v_s(z, t) = \int df g(f) u_s(z, f) e^{-2\pi i f t} \quad (6)$$

the stable component of the transient field. Since the eikonal increment δS does not depend on frequency f , the stable components in the perturbed, v_s , and unperturbed, \tilde{v}_s , waveguide are related by equation

$$v_s(z, t) = \tilde{v}_s(z, t + \delta t),$$

where $\delta t = \delta S/c_0$ is a time delay which does not depend on depth z . By analogy with Eq. (3), we introduce the similarity coefficient of two transient wave fields

$$\begin{aligned} B_{\text{tr}}(v_s, \tilde{v}_s) &= \max_{\tau} \frac{|\int dz dt v_s(z, t) \tilde{v}_s^*(z, t + \tau)|}{(\int dz dt |v(z, t)|^2)^{1/2} (\int dz dt |\tilde{v}(z, t)|^2)^{1/2}} \\ &= \max_{\tau} \frac{|\int dz df u_s(z, f) \tilde{u}_s^*(z, f) |g(f)|^2 e^{2\pi i f \tau}|}{(\int dz df |u(z, f)|^2 |g(f)|^2)^{1/2} (\int dz df |\tilde{u}(z, f)|^2 |g(f)|^2)^{1/2}}, \end{aligned} \quad (7)$$

where τ compensates for the unknown time delay δt .

The above arguments suggest that a narrow beam of rays with close phase increments forms a stable component of both CW and transient wave fields. Similarity coefficients (3) and (7) of stable components associated with the same beam of rays in the perturbed and unperturbed waveguide are close to unity. Below we consider two methods of extracting stable components from the total wave field measured in an experiment or computed in a full wave numerical simulation. Application of these methods will be illustrated using the simulation of sound fields in a deep water waveguide whose model is described in the next section.

III Environmental model for numerical simulation

In numerical simulations presented below we use an environmental model with an unperturbed sound speed profile representing the canonical (or Munk) profile [5, 6]

$$\bar{c}(z) = c_r [1 + \varepsilon (e^\eta - \eta - 1)], \quad \eta = 2(z_a - z)/B \quad (8)$$

with parameters $c_r = 1.5$ km/s, $\varepsilon = 0.0057$, $B = 1$ km, and $z_a = 1$ km. Profile $\bar{c}(z)$ is shown in the left panel of Fig. 1. The bottom depth is 5 km.

It is assumed that the weak perturbation $\delta c(r, z)$ is caused by random internal waves with statistics determined by the empirical Garrett-Munk spectrum [5]. To generate realizations of a random field $\delta c(r, z)$ we apply a numerical technique developed by J. Colosi and M. Brown [9]. In their model the perturbation has the form

$$\delta c(r, z) = c_r \frac{\mu}{g} N^2 \zeta(r, z), \quad (9)$$

where $g = 9.8$ m/s² is the gravitational acceleration, $\mu = 24.5$ is a dimensionless constant, $N(z) = N_0 \exp(-z/L)$ is a buoyancy frequency profile, $N_0 = 2\pi/(12 \text{ min}) = 0.0087$ 1/s is a buoyancy frequency near the surface, $L = 1$ km. The random function $\zeta(r, z)$ presents internal-wave-induced vertical displacements of a fluid parcel. Its realizations have been computed using Eq. (19) from Ref. [9]. We consider an internal wave field formed by 30 normal modes and assume its horizontal isotropy. Components of wave number vectors in the horizontal plane belong to the interval from $2\pi/100$ km⁻¹ to $2\pi/2$ km⁻¹. An rms amplitude of the perturbation scales in depth like $\exp(-3z/2L)$ and its surface-extrapolated value in our model is about 1 m/s. Depth dependencies of δc at three different ranges are shown in the right panel of Fig. 1.

In what follows we consider sound fields at the observation range $r = 50$ km. It is assumed that they are excited at frequencies of about 200 Hz by a point source set at depth $z_s = 0.9$ km. Only waves propagating at grazing angles $|\chi| < 12.5^\circ$ are taken into account. They are formed by rays with starting momenta $|p_0| < 0.22$.

Using a standard ray tracing technique [11], eikonal increments δS at $r = 50$ km were computed for a dense set of p_0 in 400 realizations of random waveguide. For each p_0 an interval of momenta p'_0 satisfying the condition $k^2 \langle [\delta S(p_0) - \delta S(p'_0)]^2 \rangle < 1$, where the brackets $\langle \rangle$ denote the averaging over realizations and k is the reference wavenumber at $f = 200$ Hz, was found. The width of this interval δp_0 is shown in Fig. 2 as a function of p_0 .

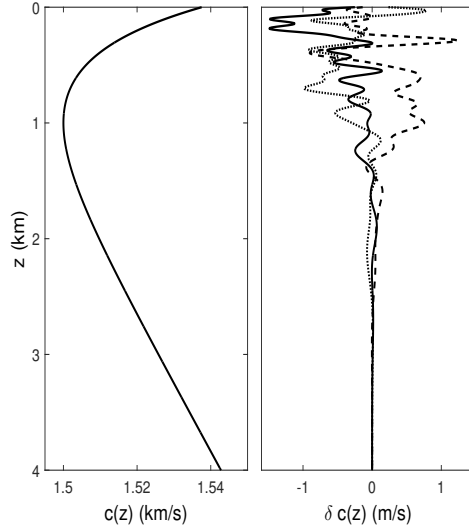


Figure 1: Unperturbed sound speed profile (left panel) and perturbation δc in vertical sections of the waveguide at three different ranges (right panel).

This plot plays a crucial role in finding stable components. For any p_0 , it allows one to find an interval $p_0 \pm \delta p_0/2$ defining a beam of rays with close phase increments at the observation range.

IV Construction of stable components from coherent states

In this section we propose a method for extracting a stable component formed by a narrow beam of rays from the total wave field. It is based on the formalism of coherent states widely used in quantum mechanics [10].

A Ray line

Introduce the phase plane $P - Z$, where P is the momentum and Z is the depth. The arrival of a ray with starting momentum p_0 at the observation range r is depicted in this plane by a point with coordinate $P = p(r, p_0, z_s)$ and $Z = z(r, p_0, z_s)$. Arrivals of rays with different

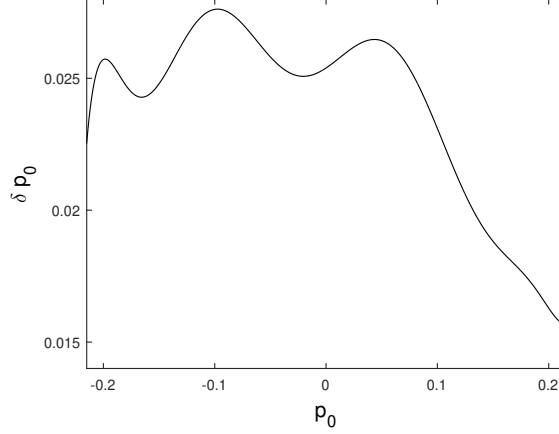


Figure 2: Estimate of δp_0 defining the interval of ray starting momenta $p_0 \pm \delta p_0/2$ corresponding to paths whose random phase increments at frequency 200 Hz remain close at 50-km range.

p_0 form a curve which we shall call the ray line. Figure 3 shows the ray line at 50-km range computed for the unperturbed waveguide described in Sec. III.

A beam of rays with starting momenta from interval $p_0 \pm \delta p_0/2$ forms a segment of the ray line. Two examples of such segments are shown in Fig. 3 by thick lines. Segments 1 and 2 are formed by rays with starting momenta close to $p_0 = -0.0975$ and $p_0 = 0.149$, respectively. Figure 2 allows one for a given p_0 to find a maximum value of δp_0 for which rays forming the segment still have close phase increments at the observation range and, hence, they still form a stable component of the total field. For Segments 1 and 2 these values of δp_0 are 0.025 and 0.018, respectively. Beams of rays forming Segments 1 and 2 with these δp_0 's are shown in Fig. 4.

B Coherent states

A coherent state associated with a point μ of the phase plane with coordinates (P, Z) is described by function

$$Y_\mu(z) = \frac{1}{\Delta_z} \exp \left[ikP(z - Z) - \frac{\pi(z - Z)^2}{\Delta_z^2} \right]$$

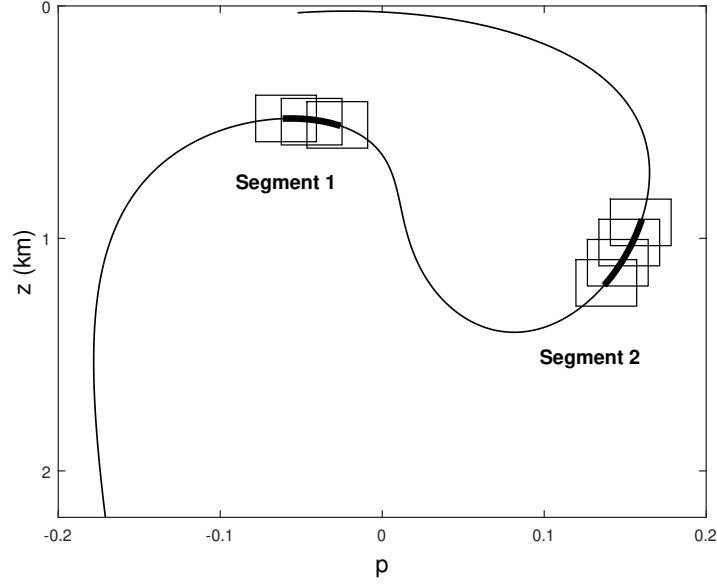


Figure 3: Ray line at 50-km range (thin solid line). Segments 1 and 2 are shown by thick solid lines. Areas covered by rectangles strung on the ray line represent fuzzy versions of Segment 1 and 2.

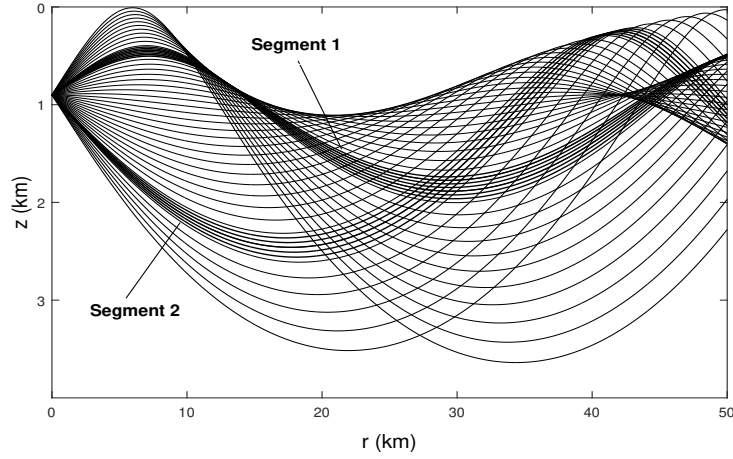


Figure 4: Fan of rays escaping a point source set at 0.9 km. Ray paths forming Segments 1 and 2 in Fig. 3 are plotted denser and shown by thicker solid lines, than other paths.

$$= \frac{1}{2\pi k} \int dp \exp \left[-\frac{\pi (p - P)^2}{\Delta_p^2} + ikp(z - Z) \right], \quad (10)$$

where Δ_z and $\Delta_p = \lambda/\Delta_z$ are the scales of this state along the axes Z and P , respectively, $\lambda = 2\pi/k$ is the reference wavelength. Function $Y_\mu(z)$ can be interpreted as a vertical section of a Gaussian wave beam of width Δ_z arriving at the observation range at grazing angle $\chi = \arcsin P$.

In quantum mechanics wave functions $Y_\mu(z)$ represent quantum states with minimum uncertainty [10]. In the analogy with quantum mechanics k^{-1} plays the role of Planck constant.

Functions $Y_\mu(z)$ satisfy the condition

$$C \int d\mu Y_\mu(z) Y_\mu^*(z') = \delta(z - z'), \quad (11)$$

where $d\mu = dPdZ$ and $C = \sqrt{2}\Delta_z/\lambda$. They form a complete system of functions and an arbitrary function $u(z)$ can be represented in the form of expansion

$$u(z) = C \int d\mu a_\mu Y_\mu(z), \quad (12)$$

where

$$a_\mu = \int dz u(z) Y_\mu^*(z). \quad (13)$$

It should be emphasized that coherent states Y_μ are not orthogonal. Their scalar product is

$$\begin{aligned} \int dz Y_{\mu_1}(z) Y_{\mu_2}^*(z) &= \frac{1}{\sqrt{2}\Delta_z} \\ &\times \exp \left[-\pi \left(\frac{(P - P_1)^2}{2\Delta_p^2} + \frac{(Z - Z_1)^2}{2\Delta_z^2} \right) + \frac{ik}{2}(P_1 + P)(Z_1 - Z) \right], \end{aligned} \quad (14)$$

where $\mu_1 = (P_1, Z_1)$, $\mu_2 = (P_2, Z_2)$. Due to the non-orthogonality of coherent states the choice of coefficients a_μ in expansion (12) is ambiguous and formula (13) used throughout the present paper gives only one of the possible options.

C Stable component associated with a segment of the ray line

Function $Y_\mu(z)$ describes a component of the total wave field associated with point μ of the phase plane. According to Eqs. (10) and (13), it is formed mainly by contributions from

rays whose arrivals are depicted by points of the plane $P - Z$ located in a rectangle with sizes $\Delta_p \times \Delta_z$ centered at point μ .

A component of the total field associated with a segment, we will determine by the expression

$$u_a(z) = C \int d\mu W(\mu) a_\mu Y_\mu(z), \quad (15)$$

where $W(\mu)$ is a weight function equal to unity on the segment and rapidly decays outside it. Equation (15) can be rewritten in the form

$$u_a(z) = \int dz' \Xi_a(z, z') u(z'), \quad (16)$$

where

$$\Xi_a(z, z') = C \int d\mu W(\mu) Y_\mu(z) Y_\mu^*(z') \quad (17)$$

is a function which does not depend on a particular realization of $u(z)$ and defines a projection onto a stable component.

So defined, the stable component $u_a(z)$ is formed mainly by contributions of rays from an area of the phase plane covered by $\Delta_p \times \Delta_z$ rectangles strung on the segment. We will call this area the fuzzy segment.

Component $u_a(z)$ can be evaluated for any segment of the ray line. But according to arguments presented in Sec. II, it is stable only if the segment includes rays with close phase increments. To satisfy this condition, besides the smallness of interval δp_0 it is necessary to select such scales Δ_p and Δ_z that the fuzzy segment is not intersected by other parts of the ray line. Since the scales Δ_p and Δ_z are connected by the uncertainty relation $\Delta_p \Delta_z = \lambda$ the latter requirement can be fulfilled only at short ranges where the adjacent portions of the ray line are spaced far enough apart or/and at a short enough wavelength λ .

For Segments 1 and 2 shown in Fig. 3 the appropriate scales at a frequency of 200 Hz can be easily selected. Figure 3 shows the fuzzy segments constructed for $\Delta_z = 0.2$ km and $\Delta_p = 0.038$. These scales will be used in our simulation for the evaluation of stable components.

The component of the transient wave field associated with a given segment, $v_a(z, t)$, is synthesized from components of monochromatic fields associated with the same segment at different frequencies f , $u_a(z, f)$ (cf. Eq. (5)):

$$v_a(z, t) = \int df g(f) u_a(z, f) e^{-2\pi i f t}. \quad (18)$$

V Construction of stable components from local eigenfunctions of the waveguide

Consider an alternative method for forming the component of wave field associated with a given segment of the ray line. It is based on the use of mode representation of the wave field, that is, on the expansion of the wave field in local eigenfunctions of the Sturm-Liouville problem [6, 11]. Since, as in the preceding section we consider the wave field at a fixed observation range, the argument r in all functions describing the wave field and the medium will be omitted for short.

Let us exploit the expansion of a monochromatic wave field $u(z)$ in orthonormal local eigenfunctions of the unperturbed waveguide $\varphi_m(z)$:

$$u(z) = \sum_{m=1}^M a_m \varphi_m(z), \quad a_m = \int dz u(z) \varphi_m(z), \quad (19)$$

where M is the number of propagating modes [6, 11, 12]. In the WKB approximation the m -th eigenfunction is determined by parameters of the reference ray whose turning depths z_{\min} и z_{\max} coincides with the turning depths of the m -th mode. For simplicity we restrict our attention to modes with both turning depths within the water bulk. Momentum of the reference ray corresponding to the m -th mode at depth z is

$$p_m(z) = \sqrt{n^2(z) - k_m^2/k^2}, \quad (20)$$

where k_m is the eigenvalue of the Sturm-Liouville problem (or the horizontal propagation constant) determined by the quantization rule [6, 11]

$$k \int_{z_{\min}}^{z_{\max}} dz p_m(z) = \pi(m - 1/2). \quad (21)$$

In the phase plane $P - Z$, the trajectory of reference ray represents an oval formed by lines $P = \pm p_m(Z)$. Examples of such ovals are shown in Fig. 5

The m -th eigenfunctions can be presented as [6, 7]

$$\varphi_m(z) = \varphi_m^+(z) + \varphi_m^-(z), \quad (22)$$

where

$$\varphi_m^\pm(z) = Q_m(z) \exp \left[\pm i k \int_{z_{\min}}^z dz' p_m(z') \mp i\pi/4 \right], \quad (23)$$

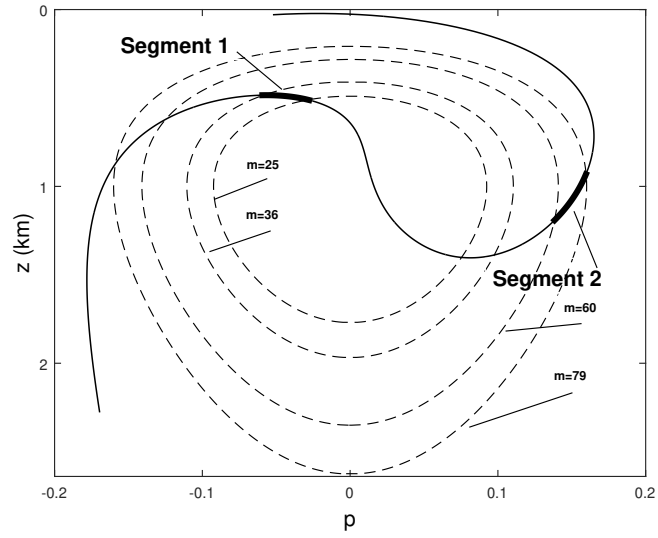


Figure 5: Thin solid line and segments of thick solid lines show the same ray line and Segments 1 and 2 as in Fig. 3. Dashed lines depict the ovals corresponding to some normal modes whose numbers are indicated next to the lines.

$Q_m(z) = [D_m \tan \chi_m(z)]^{-1/2}$, D_m is the cycle length of the reference ray and $\chi_m(z) = \arcsin(p_m(z)/n(z))$ is its grazing angle at depth z . According to Eqs. (22) and (23) the m -th mode represents the superposition of two Brillouin waves whose grazing angles at horizon z are $\pm\chi_m(z)$.

Take a segment of the ray line. If the oval corresponding to the m -th mode intersects it at point (P, Z) , then $|P| = p_m(Z)$. It means that a component of the total wave field formed by rays with momenta close to P at depths close to Z in term of modal representation is formed by Brillouin waves of modes with numbers close to m . This fact suggests an alternative representation of the field component associated with a given segment. We define this component as a superposition of Brillouin waves corresponding to a group of modes whose ovals intersects the segment. The number of modes in the group and the number of central mode denote Δ_g and m_c , respectively. Notice that the parts of the phase plane associated with a single mode and with a single coherent state have different shapes but the same area equal to λ [13].

Figure 5 shows the same ray line as in Fig. 3 with the same Segments 1 and 2 marked by thick lines. Dashed curves present the ovals which pass near the endpoints of the segments. It is seen that for Segment 1 $\Delta_g = 12$, $m_c = 31$, and for Segment 2 $\Delta_g = 20$, $m_c = 70$.

The applicability of Eq. (23) for the Brillouin waves is restricted by the fact that it fails in the vicinity of mode turning depths. But we can easily avoid the use of this analytical expression. Our task is to sum up the components of normal modes propagating at grazing angles corresponding to momenta P of points belonging to the segment. Such component of the m -th mode denote $\Phi_m(z)$. Points of the segment cover an interval of momenta whose width denote by ΔP . The central moment of this interval denote P_c . Function $\Phi_m(z)$ can be found by formula

$$\Phi_m(z) = \frac{\lambda}{\Delta P} \int dz' \varphi_m(z') \exp \left[ikP_c(z - z') - \frac{\pi(\Delta P)^2(z - z')^2}{\lambda^2} \right], \quad (24)$$

which is convenient for numerical calculations. For points z located far from the mode turning depths $\Phi_m(z)$ is close to $\varphi_m^+(z)$ or $\varphi_m^-(z)$.

Based on the foregoing, we propose an alternative to Eq. (15) expression for a field component associated with a given segment

$$u_b(z) = \sum_m W_m a_m \Phi_m(z), \quad (25)$$

where

$$W_m = \exp \left(-\pi \frac{(m - m_c)^2}{\Delta_g^2} \right), \quad (26)$$

which will be tested in numerical simulation. Although function $u_b(z)$ is formally determined at any depth z , the field component is determined only within a depth interval slightly exceeding the interval covered by the segment.

Using Eq. (19), we rewrite Eq. (25) in a form similar to Eq. (16)

$$u_b(z) = \int dz' \Xi_b(z, z') u(z'), \quad (27)$$

where

$$\Xi_b(z, z') = \sum_m W_m \Phi_m(z) \varphi_m(z'). \quad (28)$$

Functions $u_a(z)$ and $u_b(z)$ describe field components formed by rays from approximately the same area of the phase plane. Therefore it is natural to expect that these functions should be close which means the closeness of functions $\Xi_a(z, z')$ and $\Xi_b(z, z')$, as well. In the next section it will be shown in numerical simulation that this is true.

A component of the transient wave field associated with a given segment, $v_b(z, t)$, can be synthesized from components of monochromatic fields at different frequencies f , $u_b(z, f)$, in the same manner as it is described in Sec. C for a component constructed from coherent states.

VI Numerical evaluation of stable components

In this section the existence of stable components is demonstrated in numerical simulation. We evaluate and study stable components associated with the two segments of ray line shown in Figs. 3 and 5. The component which is constructed from coherent states will be called the CS component, while the other one constructed from the Brillouin waves will be called the modal component.

A Monochromatic sound field

Monochromatic sound field at a frequency of 200 Hz excited by a point source set at a depth of 0.9 km was computed in 100 realizations of random waveguide describe in Sec.

III. Stable components of the total field associated with Segments 1 and 2 were evaluated in each realization. CS component, that is, function $u_a(z)$, was evaluated with scales Δ_z and Δ_p indicated in Sec. C. Modal component, that is, function $u_b(z)$, was evaluated with parameters m_c and Δ_g indicated in Sec. V. Both components for each segment were found in a depth interval from $z_1 - \Delta_z/2$ to $z_2 + \Delta_z/2$, where z_1 and z_2 are minimal and maximal depths of segment points. For Segment 1 this interval spans from 0.38 to 0.62 km, and for Segment 2 from 0.86 to 1.3 km.

CS component is computed by formulas (16) and (17) with the weight function

$$W(P, Z) = \max_{p'_0 \in p_0 \pm \delta p_0/2} \exp \left[-4\pi \left(\frac{(P - p(p'_0, z_s, r))^2}{\Delta_p^2} + \frac{(Z - z(p'_0, z_s, r))^2}{\Delta_z^2} \right) \right]. \quad (29)$$

The integration in Eq. (17) goes over a narrow neighborhood of the ray line representing a part of the fuzzy segment.

Sound field excited by a point source at a frequency of 200 Hz was computed by the method of wide angle parabolic equation [11] for 100 realizations of perturbation δc . Depth dependencies of the sound fields for different δc at the observation range 50 km are presented by functions $u_n(z)$, $n = 1, \dots, 100$. Function $u_1(z)$ describe the sound field in the unperturbed waveguide ($\delta c = 0$). CS and modal components presented by functions $u_{a,n}(z)$ and $u_{b,n}(z)$, respectively, are computed for each $u_n(z)$. Figure 6 presents the amplitudes of stable components $|u_{a,n}(z)|$ (upper panel) and $|u_{b,n}(z)|$ (middle panel) associated with Segment 1 for six realizations of random waveguide and the amplitude of the total field within the same depth interval for the same realizations of the waveguide (lower panel). The depth dependencies of amplitudes $|u_{a,n}(z)|$, $|u_{b,n}(z)|$ and $|u_n(z)|$ for the Segment 2 look similarly (not shown).

In order to quantify the stability of CS and modal components we evaluated similarity coefficients (3) for realizations of these components in the perturbed and unperturbed waveguide. Upper panel of Fig. 7 shows similarity coefficients $B_{cw}(u_{a,n}, u_{a,1})$ (circles) and $B_{cw}(u_{b,n}, u_{b,1})$ (asterisks) for Segment 1. Points depict similarity coefficients $B_{cw}(u_n, u_1)$ for the total field within the depth interval where the stable components are defined. It is seen that both CS and modal components are indeed more stable than the total field.

To check the assumption on the closeness of CS and modal component made in Sec. V, the similarity coefficient $\alpha = B(u_{a,n}, u_{b,n})$ was computed for each realization of perturbation.

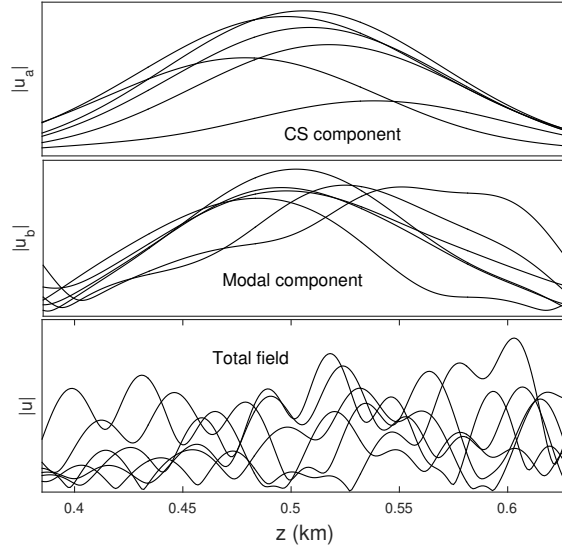


Figure 6: Amplitudes of CS components (upper panel), modal components (middle panel), and total fields (lower panel) for six realizations of perturbation δc . CS and modal components are associated with Segment 1 of the ray line.

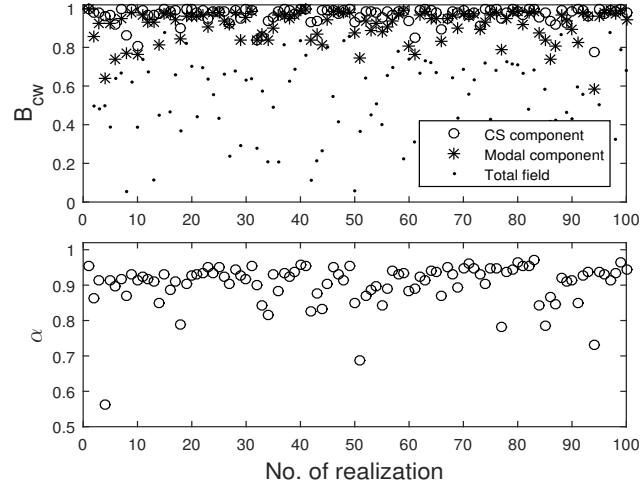


Figure 7: Stability of field components associated with Segment 1. Upper panel: similarity coefficient of CS components (circles), modal component (asterisks), and total field (points) in the perturbed and unperturbed waveguide. Lower panel: similarity coefficient of CS and modal components in the same realization of random waveguide.

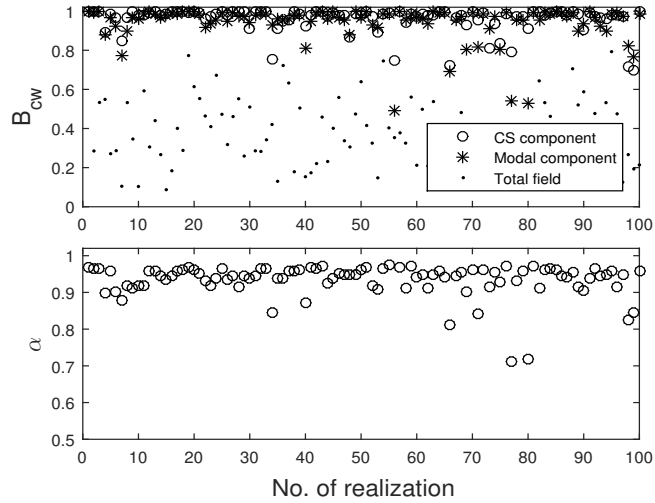


Figure 8: The same as in Fig. 7, but for field components associated with Segment 2.

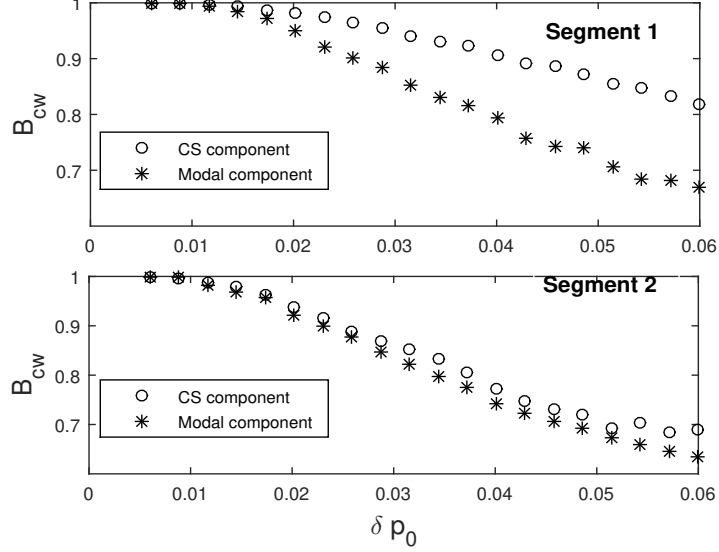


Figure 9: Upper panel: similarity coefficients for CS (circles) and modal (asterisks) components associated with Segment 1 in the perturbed and unperturbed waveguide as functions of interval δp_0 . Lower panel: the same for components associated with Segment 2. The similarity coefficients are averaged over 100 realization of random waveguide.

Consistent with our expectation, the values of all these coefficients shown in the lower panel of Fig. 7 are rather large. Similar results are obtained for Segment 2 (see Fig. 8).

As it has been indicated in Sec. C, although CS and modal components are defined for any parameter δp_0 defining the segment length, they are stable only for small enough δp_0 . Upper panel of Fig. 9 presents results illustrating the loss of stability of both CS and modal components associated with Segment 1 at change of δp_0 from 0.006 to 0.06. Circles and asterisks show the similarity coefficients $B_{cw}(u_{a,n}, u_{a,1})$ and $B_{cw}(u_{b,n}, u_{b,1})$, respectively, averaged over 100 realizations of perturbation as functions of δp_0 . Similar results for the CS and modal components associated with Segment 2 are presented in the lower panel. Let us recall that according to Fig. 2 the maximum values of δp_0 for which the field components associated with Segments 1 and 2 are expected to be stable are about 0.025 and 0.018. This agrees with what we see in Fig. 9: the decrease of similarity coefficient in the upper panel begins at $\delta p_0 \simeq 0.02$ and in the lower panel at $\delta p_0 \simeq 0.015$.

B Transient sound field

Consider a point source emitting sound pulse $s(t) = \exp(-\pi t^2/\tau_0^2 - 2\pi i f_0 t)$ with $f_0 = 200$ Hz and $\tau_0 = 0.03$ s. Complex amplitude of the sound field $v(z, t)$ at 50-km range calculated by formula (5) with $g(f) = \exp(-\pi \tau_0^2 (f - f_0)^2)$. To this end, monochromatic fields $u_n(z, f)$, $n = 1, \dots, 22$ at 81 discrete frequencies f uniformly distributed in the interval from 160 to 240 Hz were calculated by the method of wide angle parabolic equation for 22 realizations of perturbation δc . These data were used to synthesize functions $v_n(z, t)$ describing transient sound fields in the vertical section of the waveguide at $r = 50$ km. Index $n = 1$ indicates results obtained for the unperturbed waveguide ($\delta c = 0$). Then field components $v_{a,n}(z, t)$ and $v_{b,n}(z, t)$ associated with Segments 1 and 2 were found from $v_n(z, t)$.

Upper panel in Fig. 10 presents the distribution of field amplitude $|v_n(z, t)|$ in the plane time – depth for a particular realization of sound speed perturbation. Thin solid lines in both panels depict the timefront representing the ray arrival depth as a function of the ray travel time. Ray travel times are reckoned from r/c . Pieces of the timefront formed by rays belonging to Segments 1 and 2 are shown in bold. Lower panel represents amplitudes of CS components $|v_a(z, t)|$ associated with the Segments. They are localized near the corresponding parts of the timefronts. Distributions of amplitudes $|v_b(z, t)|$ representing modal components look similarly (not shown).

Stable components $v_a(z, t)$ associated with Segments 1 and 2 are weakly sensitive to perturbation δc : similarity coefficient $B_{\text{tr}}(v_{a,n}, v_{a,1})$ determined by Eq. (7) for both segments exceed 0.9 for all $n = 1, \dots, 22$. The same is true for coefficients $B_{\text{tr}}(v_{b,n}, v_{b,1})$.

Sound pulse $v_a(z, t)$ at a fixed depth z can be interpreted as a stable component of signal $v(z, t)$, recorded by a single hydrophone. Solid lines in Fig. 11 show pulses $|v_{a,n}(z_c, t)|$ at $z_c = 1.08$ km (central depth of Segment 2) for four realizations of perturbation δc . It is seen that these four pulses are indeed more similar to each other than total signals $|v_n(z_c, t)|$ (dashed lines) arriving at the same depth in the same realizations of the waveguide.

In order to quantify the closeness of pulses $v(z, t)$ and $\tilde{v}(z, t)$ arriving at the same depths z in different realizations of the random waveguide, by analogy with Eq. (7), we will use the similarity coefficient

$$B(v, \tilde{v}) = \max_{\tau} \frac{|\int dt v(z_c, t) \tilde{v}_c^*(z_c, t + \tau)|}{(\int dt |v(z_c, t)|^2)^{1/2} (\int dt |\tilde{v}(z_c, t)|^2)^{1/2}}$$

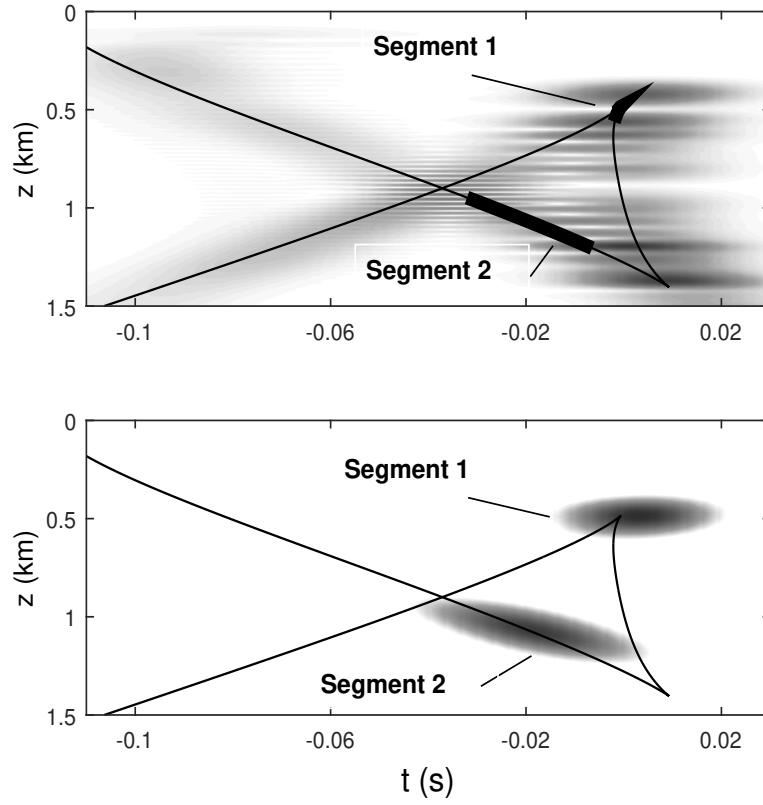


Figure 10: Amplitudes of the total field (upper panel) and its stable components associated with Segments 1 and 2 (lower panel) in the plane time – depth. The same thin line in both panels depicts the timefront. Parts of the timefront in the upper panel depicting arrivals of rays forming Segments 1 and 2 are shown in bold.

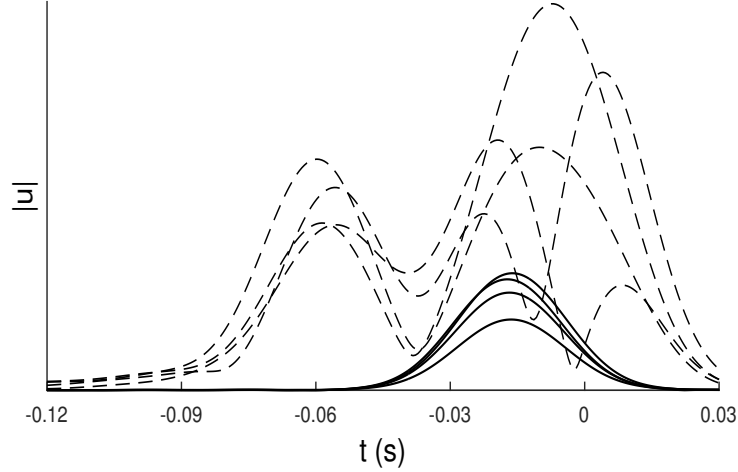


Figure 11: Sound pulses (dashed lines) at depth $z_c = 1.08$ km and their stable components associated with Segment 2 (solid lines) in four realizations of random waveguide.

$$= \max_{\tau} \frac{\left| \int df u(z_c, f) \tilde{u}^*(z_c, f) |g(f)|^2 e^{2\pi i f \tau} \right|}{\left(\int df |u(z_c, f)|^2 |g(f)|^2 \right)^{1/2} \left(\int df |\tilde{u}(z_c, f)|^2 |g(f)|^2 \right)^{1/2}}. \quad (30)$$

Upper panel in Fig. 12 depicts similarity coefficients $B(v_{a,n}, v_{a,1})$ of CS components of pulses associated with Segment 1 and received at the central depth of this segment $z_c = 0.49$ km (circles). Points show similarity coefficients of total signals received at the same horizon. Lower panel presents similar results obtained for CS components associated with Segment 2 and for total signals received at the central depth of this segment $z_c = 1.08$ km. Numerical simulation confirms stability of pulses associated with both segments. A similar result was obtained for modal components expressed by functions $v_{b,n}$ (not shown).

VII Conclusion

The procedure proposed in this paper for evaluating components of the wave field which are stable with respect to small variations of the sound speed field includes the following steps. (i) A dense fan of rays escaping the source with different starting momenta p_0 is traced in the unperturbed waveguide. (ii) On the basis of available a priori information, an ensemble of waveguides with admissible realizations of the sound speed field is constructed.

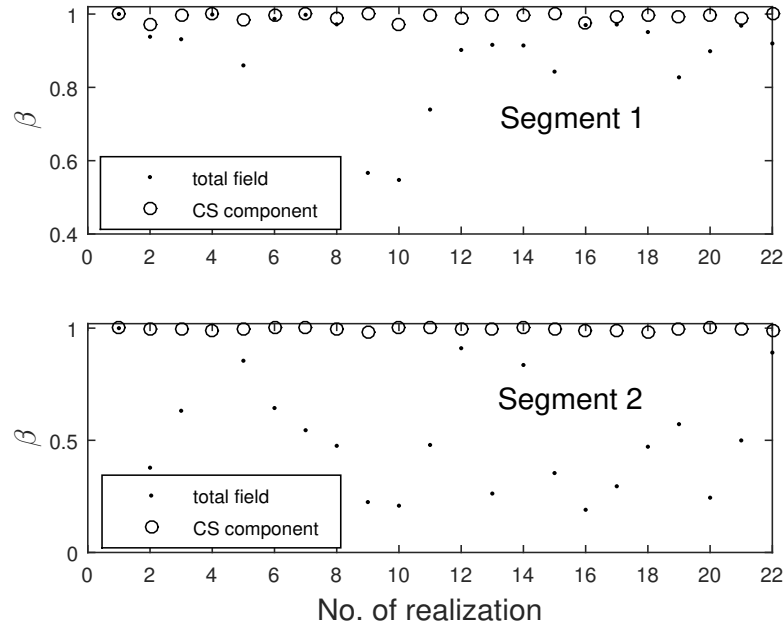


Figure 12: Similarity coefficients of signals (points) and their stable components (circles) in the perturbed and unperturbed waveguide at central depths of Segment 1 (upper panel) and Segment 2 (lower panel).

This ensemble can model not only random sound speed fluctuations but the uncertainty in parameters of the regular waveguide as well. (iii) Using Eq. (1), eikonal increments δS at the observation range are evaluated for every fan ray in every realization of the waveguide. Then, for any given frequency f and for each starting momentum p_0 such an interval δp_0 is evaluated that phase increments $k\delta S$ of rays with starting momenta from interval $p_0 \pm \delta p_0/2$ are close and these rays form a stable component of the total field. (iv) This stable component is constructed from coherent states by formulas (16) – (18), or from Brillouin waves by formulas (27) and (28). Application of this procedure is illustrated with the numerical example. We assume that a similar procedure can be applied for finding field components stable with respect to variations of the waveguide boundary.

The weak point of our approach is the fact that at present it has no rigorous justification. Stability of field components expressed by Eqs. (16) and (27), is actually only our conjecture. It is based on simple heuristic arguments formulated in Sec. II and supported by results of numerical simulation. Note that the stable component associated with Segment 1 is defined in the waveguide area with caustic (see Fig. 4), where the geometrical optics approximation fails. This and other examples not presented in this paper suggest that the approach under consideration is applicable at caustics.

Numerical simulation shows that, in spite of our assumption made in Sec. II, the amplitudes of stable components in different realizations of random waveguide may significantly differ (see Figs. 6 and 11). Weak sensitivity of functions $u_{a,b}$ and $v_{a,b}$ to sound speed fluctuations is manifested in the fact that the similarity coefficients of these components in the perturbed and unperturbed waveguide are close to unity.

The lack of rigorous justification complicates the optimal choice of scales Δ_z and Δ_p in the calculation of the CS component and scale Δ_g in the calculation of the modal component. Moreover, the proposed methods of constructing stable components may not be optimal. For example, when calculating the modal component, it may make sense to consider Δ_g , the effective number of added Brillouin waves, as a function of depth. The relationship between two representations of stable components given by Eqs. (16) and (27) is not yet studied. These issues require a further investigation which we plan to perform in next publications.

Another group of questions which is not addressed in the present paper is connected with the practical measurement of stable components (requirements for the receiving antenna) and their possible use in solving different problems of underwater acoustics (source localization, remote sensing, noise interferometry, etc). These issues, we also plan to consider elsewhere.

Acknowledgment

The work was supported by the Program “Fundamentals of acoustic diagnostics of artificial and natural media” of Physical Sciences Division of Russian Academy of Sciences, and Grants No. 15-02-04042 and 15-42-02390 from the Russian Foundation for Basic Research.

References

- [1] K.R. James and D.R. Dowling, “A method for approximating acoustic-field-amplitude uncertainty caused by environmental uncertainties”, *J. Acoust. Soc. Am.*, **124**, 1465–1476 (2008).
- [2] K.D. LePage, “Modeling propagation and reverberation sensitivity to oceanographic and seabed variability”, *IEEE J. Ocean Eng.*, **31**, 402–412 (2006).
- [3] P. Gerstoft and C.F. Mecklenbräuker, “Ocean acoustic inversion with estimation of a posteriori probability distributions”, *J. Acoust. Soc. Am.*, **104**, 808–819 (1998).
- [4] Y.-T.Lin, C.-F. Chen, and J.F. Lynch, “An equivalent transform method for evaluating the effect of water-column mismatch on geoacoustic inversion”, *J. Ocean. Eng.*, **31**, 284–298 (2006).
- [5] S.M. Flatte, R. Dashen, W.M. Munk, K.M. Watson, and F. Zakhariassen, *Sound transmission through a fluctuating ocean* (Cambridge U.P., London, 1979), Chaps. 7, 8, 11.
- [6] L.M. Brekhovskikh and Yu.P. Lysanov, *Fundamentals of Ocean Acoustics* (Springer-Verlag, New York, 2003), Chaps. 6, 10.
- [7] D. Makarov, S. Prants, A. Virovlyansky, and G. Zaslavsky. *Ray and wave chaos in ocean acoustics* (World Scientific, New Jersey, 2010), pp. 22-25.
- [8] F.J. Beron-Vera, M.G. Brown, J.A. Colosi, S. Tomsovic, A.L. Virovlyansky, M.A. Wolfson, and G.M. Zaslavsky, “Ray dynamics in a long-range acoustic propagation experiment”, *J. Acoust. Soc. Am.*, **114**, 1226–1242 (2003).
- [9] J.A. Colosi and M.G. Brown, “Efficient numerical simulation of stochastic internal-wave-induced sound-speed perturbation field”, *J. Acoust. Soc. Am.*, **103**, 2232–2235 (1998).

- [10] P. Carruthers and M.M. Nieto, “Phase and angle variables in quantum mechanics”, *Rev. Mod. Phys.*, (40), 411–440 (1968).
- [11] F.B. Jensen, W.A. Kuperman, M.B. Porter, and H. Schmidt, *Computational Ocean Acoustics* (Springer, New York, 2011), Chaps. 5,6.
- [12] L.M. Brekhovskikh and O.A. Godin. *Acoustics of Layered Media. II: Point Sources and Bounded Beams* (Springer-Verlag, Berlin, 1999), Chap. 7.
- [13] L.D. Landau and E.M. Lifshitz. *Quantum mechanics* (Pergamon Press, Oxford, 1977), Chaps. 2, 7.